Proceedings of the 2003 IEEE
International Conference on Robotics & Automation
Taipei, Taiwan, September 14-19, 2003

Experiments using a Laser-based Transducer and Automated Analysis Techniques for Pipe Inspection

Olga Duran, Kaspar Althoefer and Lakmal D. Seneviratne
email : {olga.duran,k.althoefer,lakmal.seneviratne}@kcl.ac.uk
Department of Mechanical Engineering
King's College London
Strand, London WC2R 2LS,
United Kingdom

Abstract – **This paper presents the experimental results of an automated sensor system for the inspection of tubular structures. The method is applied to the autonomous inspection of sewers overcoming the drawbacks of standard CCTV-based inspection systems. The transducer consists of a low-cost laser-based profiler attached to a standard CCTV camera. Image analysis techniques and artificial neural networks are used to automatically locate and classify the defects in the pipe using the intensity distribution in the acquired camera images. A wide range of tests using data from different types of pipes in realistic conditions have been conducted and are presented here. It is shown that the proposed inspection approach is particularly well suited to complement existing CCTV inspection systems, providing automated and reliable detection of pipe defects in the millimeter range.**

I. INTRODUCTION

Standard pipe inspection systems are based on Closed Circuit Television (CCTV) cameras in a large range of application fields such as waste pipes and drains. The CCTV method consists of a mobile, remotely-operated platform usually equipped with a color, high-resolution video camera and a lighting system. The camera platform is connected via a multi-core cable to a remote inspection station with video recording facilities situated overground. An engineer then assesses the recorded images off-line. This is a subjective and time-consuming task that considerably increases the inspection costs. Moreover, only gross anomalies are evident to the human eye, which reduces the detection of faults at early stages. Another drawback associated with those systems in these particular environments is the lack of visibility inside the pipes and the poor quality of the acquired images that hinders a complete assessment of the pipe condition and sometimes even the detection of large defects.

A number of automated inspection techniques that aim to cope with the drawbacks of CCTV have been proposed in recent years [1]. Special lighting and profilers systems have been proposed to cope with the image quality problems [1,4]. These systems usually work by projecting either a thin ring of light or successive light spots using a rotating mechanism onto the pipe wall. T. Tsubouchi and *et al* proposed a different approach using a laser spot array instead of a light ring [11]. As the platform moves through the pipe, the succession of profile measurements allows the creation of a surface map of the inner pipe wall. Geometrical changes of the pipe surface can be retrieved from the changes in the position of the ring on the acquired image using the principle of triangulation [1].

Besides image quality problems, the automation of the process has been proved to be a very important issue, and intelligent classification defect algorithms are investigated [1]. Recognition and classification of pipe surface defects from digitized video images using image analysis pattern recognition and artificial neural networks have been proposed recently [2,3]. Although those systems overcome automation-related disadvantages of human CCTV assessment, they still rely on the quality of the raw camera images.

In this paper a laser profiler is used to enhance the quality of the pipe images. Compared to previous work, the novelty here is the use of the intensity information instead of the positional deformation of the ring of light. Intelligent analysis and classification techniques are applied to the acquired images to automate the inspection process. This approach is based on detecting sharp changes in the image intensity values. Neural networks are used in a first stage for the identification of defective pipe sections, and further to classify them into types of defects. The input to the ANN is a pre-processed signal that emphasizes the differences between defective and non-defective pipe sections. The network employed is a multi-layer perceptron (MLP), trained by a backpropagation algorithm, widely used for solving classification problems [7,9].

This paper extends the research that aims at creating autonomous sensors for low-cost, self-reliant pipe inspection presented in [8]. Here a wide range of tests using data from different types of pipes are presented. It is shown that the proposed inspection approach is particularly well suited to complement existing CCTV inspection systems, providing automated detection and classification of pipe defects in the millimeter range employing a low-cost system add-on and classification algorithms with real-time capability.

II. TRANSDUCER DESCRIPTION

The transducer used here is based on a laser light generator that projects rings of light onto the pipe wall, that are then acquired by a CCD camera and stored in a PC using a frame grabber. The CCD camera is rigidly attached to the lighting system, a ring pattern diffuser driven by a 1-mW, 635nm-wavelength laser diode. The optical pattern diffuser is built from acrylic material and is used to project a pre-defined circular light pattern, lighting a confined pipe section [6]. Figure 1 shows the light path corresponding to the diffuser used in the experiments.

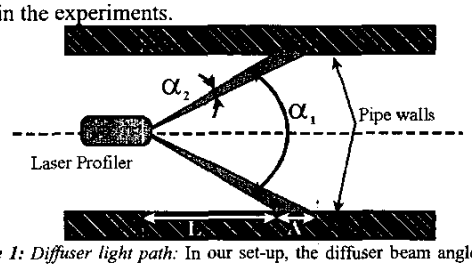

Figure 1: *Diffuser light path:* In our set-up, the diffuser beam angles were α_1=11.3°, α_2=0.2 °.

The location of the surface under investigation relative to the platform can be found by pure trigonometry, without the need for an external spatial reference. Equations 1 and 2 show the expressions for this distance and the area illuminated respectively:

$$L = \frac{R}{\tan(\alpha_1/2)} \quad , \tag{1}$$

$$A = R \cdot \left(\frac{1}{\tan(\alpha_1/2 - \alpha_2)} - \frac{1}{\tan(\alpha_1/2)}\right) \quad , \tag{2}$$

where L is the distance from the projected ring to the transducer, A is the width of the illuminated ring, and α_1 and α_2 are the diffuser angles as depicted in figure 1.

Is it noted that the projection angle (α_1) will define the distance L between the transducer and the area under investigation, while the fan angle (α_2) gives the resolution of the method. Here, a wide fan angle (α_2) is used since then a larger area is illuminated and analyzed using the same image, speeding up considerably the inspection process.

At locations of discontinuities, the intensity of the projected rings changes abruptly. These changes are due to the characteristics of the reflected light at discontinuities, where the light is scattered depending on the smoothness of the surface, but reflected according to the basic law of reflection at different angles and intensities compared to non-defective pipe images [10]. Although similar types of projection methods have been successfully used to measure pipe deflection or change of shape using the positional information in the image [1,4], the intensity data has not been used by other researchers. The additional information that can be extracted is related to local discontinuities, such as cracks or holes, which can be identified by analyzing the light intensity of the projected rings.

III. ANALYSIS TECHNIQUE OVERVIEW

An intensity extraction algorithm is used to compute the ring intensity information from the image. Instead of analyzing the raw data obtained from the transducer, first, the ring of light is identified from the image background, by applying an ellipse-fitting algorithm to each input image. This reduces significantly the computational complexity and the volume of data processed.

A. Pre-processing

The acquired camera image of the ring projection is in most cases an ellipse, although the originally generated light ring is circular. This is due to misalignments of the camera with respect to the pipe center causing the ring projection to distort into an ellipse. Here, a numerically-stable and fast algorithm is applied to fit an ellipse to the set of data points given by an edge detector [5,6,8]. The algorithm used is non-iterative and based on a least squares minimization of the algebraic distance between the data points and the ellipse [6].

B. Intensity extraction

Once the ellipse is identified, an algorithm extracts the ring intensity information from the image. The algorithm is based on a local average computation of the intensities along individual segments of the found ellipse:

$$\overline{\mu}_j = \frac{\sum_{i=0}^{255} \mu_i \cdot i}{n \cdot m} \quad , \tag{3}$$

where $\overline{\mu}_j$ is the local average of segment j, i is the gray level of a certain image point, μ_i the frequency of that gray level and the size of the scan window is given by n by m. For each window, one average intensity value is calculated using equation 3. A set of such average intensities, $\overline{\mu}_j$, with $j \in [1,2,.....P]$, represents the intensity distribution along a ring profile (figure 2).

Since the image of the ring of light is wider than one pixel, an average intensity is computed over a sliding window covering areas along the ellipse. The size of the window is defined taking into account the geometric characteristics of the projected cone of light (figure 1) and the CCD camera intrinsic parameters. As an example, the light ring for a 260mm diameter pipe covers 60mm of pipe width and 6 pixels in the pipe image.

A surface map of the inner wall of the pipe is created with successive intensity representations computed while the platform travels along the pipe (figure 3). Abrupt peaks of intensity show the location of potential pipe discontinuities such as cracks, holes or joints.

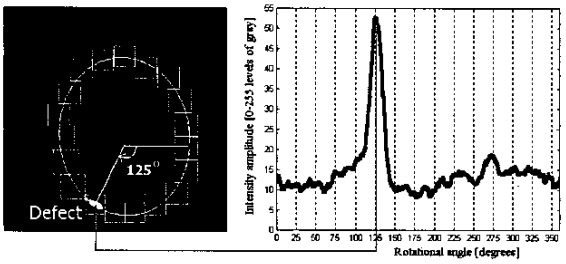

Figure 2: Intensity data extraction algorithm generating an intensity distribution for each profile; a sliding window is applied along the ellipse. The peak in the profile indicates the location of a potential discontinuity.

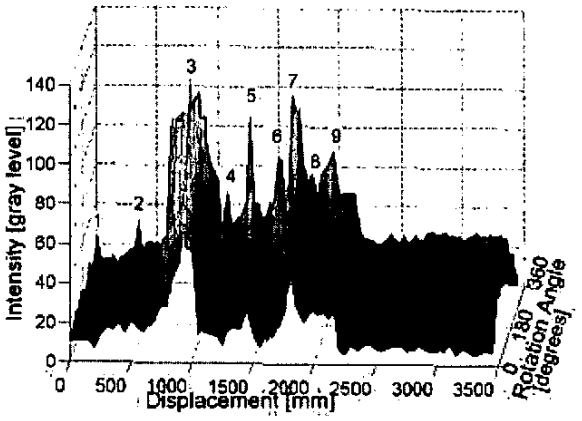

Figure 3: Surface map of a PVC pipe with an internal diameter of 260 mm. This pipe has the following incidences:1) hole; 2) hole; 3) joint between 2 pipes; 4) radial crack; 5) joint between 2 pipes; 6) obstacle; 7) joint between 2 pipes; 8,9) cracks in a rough surface.

IV. AUTOMATED DEFECT CLASSIFICATION

Artificial Neural Networks (ANN) are widely used in pattern recognition because of their ability to generalize and to respond to unexpected inputs [9]. Images usually contain unwanted, random signals (i.e. noise) in addition to the pipe interior image. Noise may be caused by a wide range of sources, such as drifts in detector sensitivity, environmental variations or platform motion. Irrelevant scene details such as surface reflectance textures are also considered as image noise. Intelligent algorithms able to learn from the real images and self-adapt to irregularities in images are needed to cope with the limitations of simple low-level vision algorithms.

Two classification stages have been used in this work. As a first step, a binary classification identifies and locates the defective profiles. Further defect classification is performed by a second classifier. The ANNs employed in both stages are based on a multi-layer perceptron (MLP) architecture. They consist of an input layer, an output layer and one hidden layer. The number of nodes per layer has been chosen using a trial and error procedure. These parameters have been validated experimentally with unseen data (see Section V). The training algorithm used in this study is the scaled conjugate gradient (SCG) algorithm which is based on backpropagation, and widely used for solving classification problems [7].

A. Binary classification

The ANN is fed with sets of pre-processed data representing pipe cross-section profiles. Even if the extracted intensity data could be used directly as input to the network, it is better to pre-process this data and create signatures in order to highlight characteristics of defective and non-defective pipe sections, and to remove non-relevant data that could interfere with the learning process and complicate the classification task. The signature generation approach used here employs a sorting algorithm [8]. The data for each pipe section is sorted by signal amplitude in descending order. Thus any defective section, having one or more intensity peaks, is converted into a monotonically decreasing sequence. A normalization step is now applied, by subtracting the intensity values at each section from the maximum intensity value. The resulting signal is a monotonically increasing sequence starting from zero (figure 4). Non-defective sections will appear as relatively flat signals. Signals representing a defective section will have a sharp slope reaching a fairly flat region at a higher amplitude [8].

The selection of network architecture and training parameters was done in a trial and error procedure. The best performance was achieved with a multi-layer perceptron with three layers: the first layer with 10 input neurons, accepting the first 10 values of the sorted signature as input, a second hidden layer with 5 neurons and one output neuron. The data used during training consists of 175 normalized signatures, corresponding to both faulty and non-faulty pipe sections. The training behavior showed that this algorithm is able to classify the training data bringing the error down to 2.7E-6 after 4000 epochs.

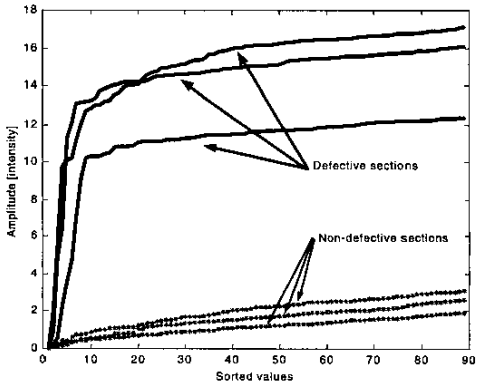

Figure 4: Normalized signature of defective and non-defective sections: Defective sections with faults at different spatial locations along the profile have similar signature.

B. *Defect classifier*

Image processing tools were used to investigate the generated surface map at locations were the binary classification indicated a potential fault. Firstly, objects were extracted from the surface map for the defective profiles (figure 9). Those objects correspond to the defect shapes, and geometrical information can be extracted from them. Here, the following geometrical attributes have been selected: length of the major axis, length of the minor axis, ratio between the axes, center of the defect, and area. The center gives the exact location of the defect, while the minor and major axis, and the ratio provide information about its shape. The area of the object measures the severity of the defect. These features are then fed into a classifier to evaluate and classify into types of defects, namely radial cracks, holes or defective joints.

The selection of network architecture and training parameters was done again by a trial and error procedure. The best performance was achieved with a multi-layer perceptron with three layers: the first layer with 3 input neurons, accepting the selected attributes as input, a hidden layer with 10 neurons and one output neuron. The data used during training consists of 50 sets of data from different faulty pipe sections.

V. EXPERIMENTAL RESULTS

A wide range of tests using data from different types of pipes and under different conditions were conducted to test the performance of the system. Experiments using pipes with different diameter, material, wall texture and color were conducted to test the behavior of the ANN to unseen different data. For each experimental case, defects of different sizes and shapes are evaluated. Holes and cracks of different sizes, from 10cm down to 2mm, were inserted in the walls of the pipe segments to simulate defects. The loose connection of two pipes simulates a defective joint. Table I shows an overview of the binary classification experiments and results obtained that are described next. Defect classification tests are also shown in Section E.

A. *Binary classification ability*

The ability of the trained network to cope with unseen data was also tested. A set of 100 normalized signatures corresponding to both faulty and non-faulty pipe sections not seen before by the ANN, but corresponding to pipes of similar characteristics to the ones used during training (diameter, material and texture), is fed to the ANN. The ANN is able to distinguish between defective and non defective sections in all 100 cases, classifying correctly with errors down to 15% (defective areas resulting in an output of less than 0.15 and non-defective in an output more than 0.85). A binary output can be obtained by converting results greater than a fixed threshold of 0.5 to "1" and the rest to "0".

Figure 5 shows the output results for pipe segments covering 3.5 meters whose signatures have not been seen during training. These results show that the network is able to identify irregularities in the data (related to defective sections), even though the data was not seen by the network beforehand. All incidences covering longitudinal cracks, radial cracks and holes are identified and can be distinguished using a fixed threshold of 0.5 except the cracks on the rough surface (defects 8 and 9 in figure 3). This is probably due to the fact that the training set did not contain signatures corresponding to rough surfaces since the training was done using PVC pipes only as shown in the first raw of Table I. An appropriate adapted threshold (e.g. 0.9) would still allow correct classification, since the network response to non-defective regions was clearly above 0.85 in most of the experiments conducted. However further pipe texture experiments are currently being carried out to evaluate the limits of the approach.

TABLE I: EXPERIMENTAL RESULTS

Experiments	Profiles	Success rate [%] with 0.5 threshold	
		Defective	Non-defective
Training environment: Gray PVC pipes, 260mm diameter, defects: small holes and cracks of mm width and up to a 10cm long	100	100	100
Test environment 1: Unseen data with similar characteristics to training data	100	100	100
Test environment 2: Pipes with rough surfaces, diameters of 260 and 330 mm; defects: small holes and joints.	50	85	100
With 0.85 threshold:		*100*	*100*
Test environment 3: Clay and PVC pipes, with internal diameter of 330/360 mm; defects: small holes and joints.	80	80	100
Defects in the cm range and larger:		*100*	*100*

B. *Pipe texture*

The system has also been subjected to pipes with particular rough surfaces, in order to see the performance of the system under harsh conditions. It is noted that the rougher the surface, the more difficult it becomes to distinguish defective areas by the naked eye as the intensity of the reflected rings is increased compared to a similar pipe with smooth walls. The result is a less contrasted image (figure 6). Decreasing the iris aperture in the CCD lens increases the contrast in the image and the defects are emphasized. Further tests with a lower iris aperture are tried in surfaces with roughness height and spacing in the millimeter range (figure 7). The outcome of this experiment shows that with selected threshold of "0.85", the algorithms are able to detect the defects and to discriminate them from the roughness of at least the same order of magnitude (Table I).

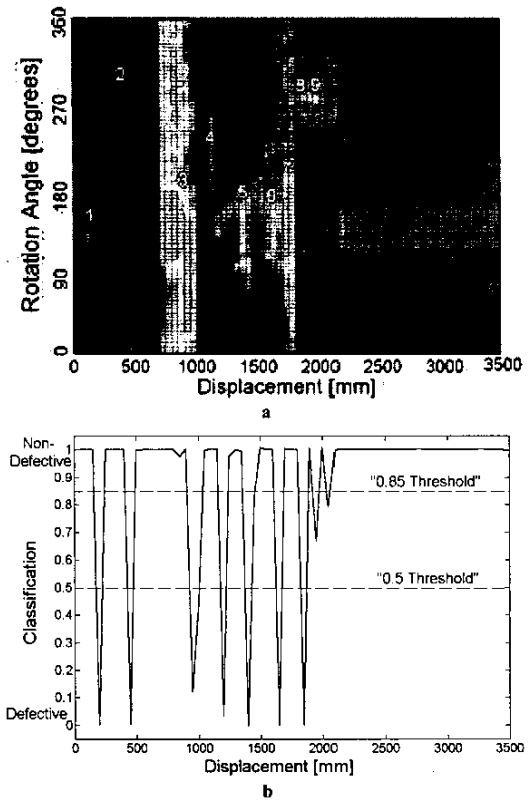

Figure 5: Classification using the NN of a PVC pipe with an internal diameter of 260 mm. a) Top view of the surface map shown in figure 3. This pipe segment has the incidences described in figure 3; b) Binary classification on defect. The values '1' or '0' correspond to non-defective and defective sections respectively.

C. *Pipe color*

Experiments with different colored pipes were also conducted. Here the intensity distribution experiences a shift in the mean intensity. As this information is treated in a differential way when generating the signatures, the response of the algorithm and the ANN is independent of the mean intensity. The tests show that apart from extremely reflective colors (e.g. white pipe walls), defects can be identified in differently colored pipes.

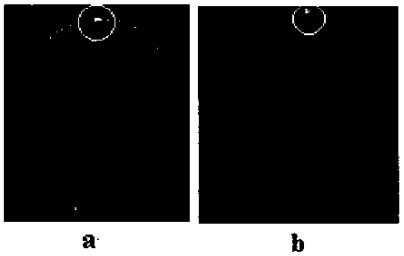

Figure 6: Reflected ring images of pipes with respectively smooth and rough walls; a) Rough walls; b) Smooth walls.

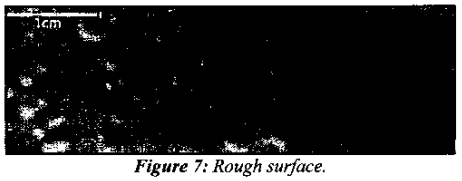

Figure 7: Rough surface.

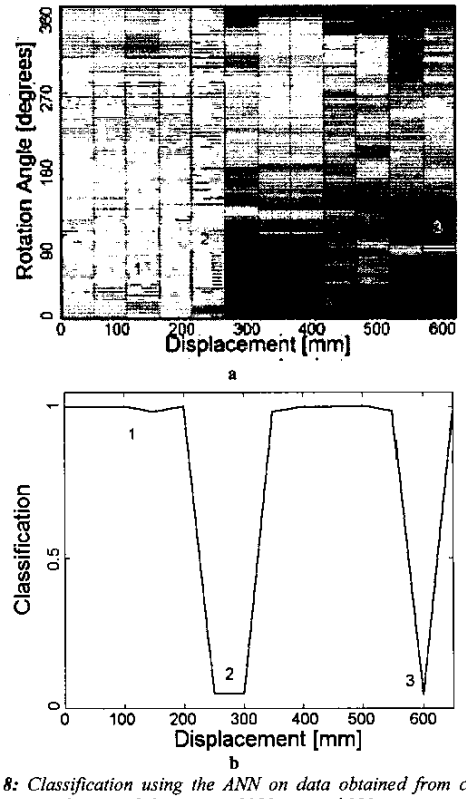

Figure 8: Classification using the ANN on data obtained from clay and plastic pipes with internal diameters of 350 mm and 330 mm respectively. a) Top view of the surface map; b) Classification using the ANN: Small holes in the millimeter range, which are not detected (1); the joint between the 2 pipes which is detected (2). A hole in the centimeter range, which is detected (3).

D. *Pipe material and size*

Tests were conducted varying pipe material and pipe diameter. PVC and clay pipe sections with inner diameters of 330 and 360 mm respectively were used. The tests show that small holes in the millimeter range are not detected, while holes in the centimeter range and joints are detected by the ANN (figure 8). This is mainly due to the fact that an increase in pipe diameter results in a dramatic increase of the distance L from the platform to the projected ring. Subsequently the resolution in the camera images decreases as the same number of pixels cover a larger area. The inspection of pipes with bigger diameters would require the use of a profiler with a higher projection angle and a higher-resolution CCD or a zoom lens, if the resolution is to be maintained.

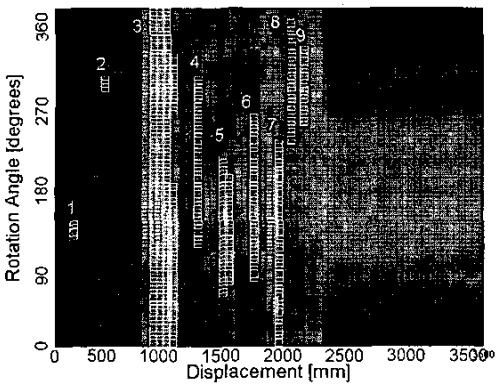

Figure 9: *Defect extraction map at defect locations.* Nine defects are identified according to the surface map shown in figures 3 and 5. The white squares are the output of the object extraction algorithm where nine objects were identified.

E. Defect classification

Surface maps whose profiles have been found defective by the binary classifier are analyzed and defects are extracted. Figure 9 shows the object extraction result for the surface map shown in figure 3, where nine objects are identified.
As an example, Table II shows the selected attributes, namely, area of the defect, length of the major axis (MA), length of the minor axis (ma) and ratio between the axis (ma/MA), related to the surface map in figures 3 and 5 and extraction map in figure 9. These features are then passed to the ANN that classifies into the defects: radial cracks, holes or defective joints. An itemized output of "1", "0" and "-1" is obtained by converting results using fixed "0.5" and "-0.5" thresholds. Experimental tests proved that the major, minor axis and their ratio were sufficient to achieve the classification. The results using these three attributes are also shown in Table II.

TABLE II: CLASSIFICATION RESULTS

N	Area	MA	ma	ma/MA	Target	ANN o/p	Classification
1	4	5	1	0.25	Hole	0.003	Hole
2	3	3	1	0.33	Hole	0.008	Hole
3	226	103	3	0.03	Joint	- 0.99	Joint
4	44	51	1	0.02	Crack	0.98	Crack
5	64	38	2	0.06	Joint	- 0.99	Joint
6	43	50	1	0.02	Obstacle	0.99	Crack
7	54	62	1	0.02	Joint	-0.9013	Joint
8	32	37	1	0.03	Crack	1	Crack
9	20	23	1	0.05	Crack	0.99	Crack

These results showed that the classifier identifies correctly holes, cracks and defective joints. Obstacles were wrongly identified as cracks since the ANN was not trained to classify such faults. In general, the classifier can identify holes and radial cracks. It is noted that in some cases, it does not differentiate between cracks and defective joints. Further selection of attributes has to be investigated to achieve a robust discrimination, to incorporate other defect targets such as obstacles and longitudinal cracks and also to give a measure of fault severity.

VI. CONCLUSIONS

In this paper, experimental tests of a laser-based transducer and classification method to inspect tubular structures are presented. The method is developed for sewer inspection, but the techniques can be applied to most pipe inspection problems. An overview of the used transducer and analysis techniques are given. The transducer is based on a laser ring generator attached to a standard CCTV camera. The method consists of analyzing the intensity levels of the projected rings viewed by the camera. An artificial neural network is used to automatically locate the defects. Experiments to validate this new analysis method under harsh conditions using different types of pipes have been conducted and results are shown here. It is noted that the resolution of the method is inversely proportional to the pipe diameter, resulting in defect detection capabilities in the millimeter range for 260mm diameter pipes. The system has also been subjected to pipes with particular rough walls, where defects were also successfully identified. Finally, the classification into defect categories using features extracted from a generated surface map is conducted using image processing and an ANN. Results show that the ANN can identify holes, radial cracks and defective joints.

REFERENCES

[1] Duran, O. Althoefer, K. and Seneviratne, L.D., "State of the art in sensor technologies for sewer inspection", IEEE Sensors journal, Volume 2, Issue 2, April 2002, pp 73-81.

[2] Moselhi, O. Shehab-Eldeen, T. "Classification of defects in sewer pipes using neural networks". Journal of infrastructure systems 6, 3, pp 97-104, 2000.

[3] Sinha, S.K.; Karray, F. "Classification of underground pipe scanned images using feature extraction and neuro-fuzzy algorithm" IEEE Transactions on Neural Networks, Volume: 13 Issue: 2, pp 393 –401, March 2002.

[4] Kirkham, R. Kearney, PD, Rogers, KJ., "PIRAT – A system for quantitative sewer pipe assessment", International Journal of Robotics Research, Vol. 19, pp 1033-1053, 2000.

[5] Gonzalez R.C. Digital Image Processing. Addison-Wesley, MA, 1987.

[6] Halir, R. Flusser J.: "Numerically stable direct least squares fitting of ellipses". The Sixth International Conference in Central Europe on Computer Graphics and Visualization, Plzeò, pp. 125-132, 1998.

[7] Moller, M. F., "A scaled conjugate gradient algorithm for fast supervised learning," Neural Networks, Vol. 6, pp 525-533, 1993.

[8] Duran, O. Althoefer, K. and Seneviratne, LD, "Automated Sewer Inspection Using Image Processing and a Neural Classifier ", in Proceedings of International Joint Conference in Neural Networks (IJCNN), Volume 2, pp 1126-1131, 2002.

[9] Haykin, S. Neural Networks. A Comprehensive Foundation. Macmillan College Publishing Company, NY, 1994.

[10] Alonso, M. Finn, E.J.: Fundamental University Physics, Vol.1&2, Addison-Wesley, Reading, Mass. 1983.

[11] Tsubouchi, T. Takaki, S. Kawaguchi, Y. and Yuta, S., "A straight pipe observation from the inside by laser spot array and a TV camera," Proc. of IEEE Int. Conf. on Intelligent Robots and Systems (IROS), pp. 82-87, 2000.